Study on the Effect of Irradiance Variability on the Efficiency of the Perturb-and-Observe Maximum Power Point Tracking Algorithm

Victor Arturo Martinez Lopez *,† , Ugnė Žindžiūtė † , Hesan Ziar * , Miro Zeman and Olindo Isabella

Photovoltaic Materials and Devices, Delft University of Technology, 2628 CD Delft, The Netherlands
* Correspondence: V.A.MartinezLopez@tudelft.nl (V.A.M.L.); H.Ziar@tudelft.nl (H.Z.)
† These authors contributed equally to this work.

Abstract: Irradiance variability is one of the main challenges for using photovoltaic energy. This variability affects the operation of maximum power point trackers (MPPT) causing energy losses. The logic of the Perturb-and-Observe MPPT algorithm is particularly sensitive to quick irradiance changes. We quantified the existing relation between irradiance variations and efficiency loss of the logic of the Perturb-and-Observe MPPT algorithm, along with the sensitivity of the MPPT to its control parameters. If the algorithm parameters are not tuned properly, its efficiency will drop to nearly 2%. Irradiance variability causes a systematic energy loss of the algorithm that can only be quantified by ignoring the hardware components. With this, we aim to improve the energy yield estimation by providing an additional efficiency loss to be considered in the calculations.

Keywords: maximum power point tracking (MPPT); solar power generation; energy efficiency; perturb-and-observe (P&O)

1. Introduction

In 2021, the world generated 821 TWh of electricity from solar PV. This considerable growth of PV generation of 23% is still not enough to meet the growing goals of 24% yearly in order to reach the 6970 TWh of solar generation in 2030. Because of this, additional efforts are needed to increase PV production worldwide [1].

A wafer-to-system analysis [2] shows that most of the energy losses occur at a cell level. The commercial crystalline silicon solar cells have efficiencies reaching 25% [3] while commercial modules have an average efficiency of 20.4% at Standard Test Conditions (STC) [3]. The rest of the losses in the PV system efficiency chain are related to the weather conditions of the site such as the irradiance, temperature and light spectrum effects [2]. Finally, the Balance-of-System components, which support the PV modules, also contribute to losses. Of these, the power converter accounts for the majority of the losses [2].

Based on this analysis, there are several options for increasing the PV system efficiency. Multi junctions can boost the efficiency of PV cells. For example, using perovskites with silicon can boost the cell's efficiency up to 31.25% [4]. At a module level, improving the module's performance under partial shading conditions also leads to an increase in efficiency. A novel way to achieve this is by reconnecting blocks of cells of the PV module in series or parallel depending on the shading pattern of the module [5]. Moving to the system domain, switching from simple converter topologies such as the buck or boost converters, with efficiencies ranging around 97%, to more advanced designs that employ soft switching techniques, also leads to better efficiency. In addition, the way that different converters are connected in the system opens a window of opportunity for efficiency improvement [6]. The power extracted from PV modules can be maximized by employing maximum power point trackers (MPPT). Their algorithms act upon the power converter to ensure that the PV module delivers the highest possible power, increasing the system's efficiency [6].

Multiple techniques can be found to deal with this topic that span over different degrees of complexity, efficiency, and objectives. For an overview of the MPPT methods, the reader is referred to the work of Karami et al. [7], with a classification of 40 MPPT methods into five categories based on their operating principle. Many other literature reviews list MPPT methods (e.g., [8,9]). In addition, in many of these, the Perturb-and-Observe is one of the first to appear.

This algorithm is one of the most widely used techniques for a PV module's maximum power point (MPP) tracking [9]. The reason behind its popularity is the simplicity of its logic [10]. It is so simple that it can be implemented in a very accessible embedded board such as the Arduino Nano [9] or even without a microcontroller by means of an analog circuit [7,9,11]. The algorithm applies a small voltage *Perturbation* to modify the module's operating point. Then, it *Observes* the resultant power. Depending on the sign of the power change, the next voltage perturbation will either increase the voltage or reduce it. In this way, the operating point will climb along the power–voltage (P–V) curve towards the maximum power point. Under constant irradiance and steady-state operation, the operating power will constantly swing around the theoretical maximum power point. With variable irradiance, the P–V curve of the module is continuously changing. Hence, the operating point occurs on different curves at each perturbation. This causes a potential problem for the algorithm that can become *confused*, setting an operating point different than the MPP and thereby leading to energy loss [8,10,12].

Figure 1 shows an example. Suppose that the algorithm starts at the maximum power point of the bottom P–V curve (marked with a diamond). The perturbation is positive and the observed power (with no irradiance change) is supposed to be lower, which, in turn, should result in the algorithm decreasing the voltage. Nonetheless, because the irradiance starts to increase, the observed power is now on another P–V curve with a higher value than before. In this scenario, if the irradiance keeps on increasing, the algorithm keeps on increasing the voltage as well. This confusion results in the tracking drifting away from the MPP of every curve and continues until the observed power is lower than the previous. At that moment, the algorithm operates correctly and starts climbing back to the MPP (even with the still increasing irradiance).
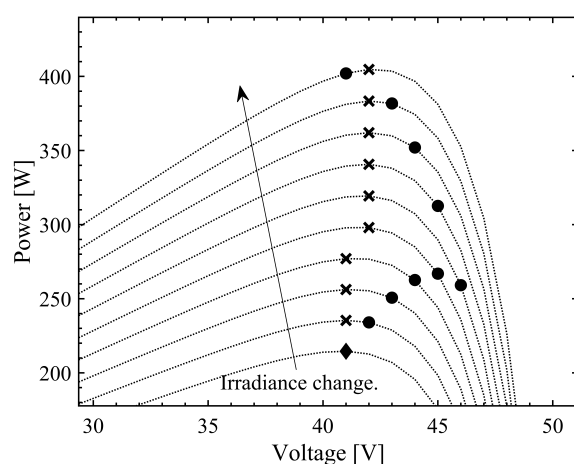
Figure 1. Example of the P&O confusion when the irradiance increases. The circles indicate the tracking points. The 'x' denotes the maximum power point at each P–V curve, and the diamond marks the starting point.

The P&O algorithm has two parameters that define its operation and can be tuned for optimization. The first is the sampling time, T_a. It determines how often a perturbation will be made. The second is the amplitude of the perturbation given by the voltage step ΔV. This parameter specifies the magnitude of the change in power that the module experiences (ΔP) [12]. The magnitude of the resultant power as a consequence of a voltage perturbation, its direction (increasing vs. decreasing voltage steps) as well as the power change caused

by irradiance (ΔP_G) determine whether the algorithm will track in the correct direction or not [12,13]. When the algorithm is decreasing the voltage to reach the MPPT, it will not be confused if Equation (1) is fulfilled [12,13]:

$$|\Delta P| < |\Delta P_G|. \tag{1}$$

When the algorithm increases the voltage to reach the MPPT, the inequality of Equation (1) is reversed [13].

The method presented here corresponds to the most basic version of the P&O algorithm, where the sampling time and perturbation step are fixed. There are many modifications to this algorithm that aim to improve its performance but maintain the basic operating principle. Many of these improvements to the basic P&O algorithm are based on dynamically changing the algorithm's parameters [13]. For example, the perturbation step is larger during the hill-climbing process but then reduced in size when the algorithm reaches the MPP leading to increased tracking speed and small steady-state oscillations [7]. We analyzed the P&O algorithm because of its simplicity and widespread use. Without losing generalization, we will only focus on the most basic form of the P&O algorithm.

1.1. Irradiance Variability

"Variability" describes how often a quantity changes in time. High variability indicates frequent and significant changes, while low variability is linked to gradual changes.

When describing the Global Horizontal Irradiance (GHI), irradiance with high variability in a given period will exhibit high *dispersion*. Because of this, the standard deviation, as a measure of dispersion, is used to quantify irradiance variability.

Variability is more evident when considering the *differences* between two consecutive irradiance measurements. These differences are close to zero for gradual changes, hence low *dispersion*. The first variability metric, V, is then a measure of the dispersion of the changes in irradiance within a certain period. Mathematically, $V = \sigma(\Delta G)$, where G represents the measured irradiance (GHI).

To remove the effect of day–night cycles and allow the study of variation caused by clouds, the clearness index k_t (2) can be used [14]. It relates the measured irradiance G against the modeled irradiance at the top of the atmosphere (extraterrestrial irradiance, G_{ext}) [15]:

$$k_t = \frac{G}{G_{ext}} \tag{2}$$

If extraterrestrial irradiance in (2) is replaced with the clear-sky irradiance, the clear-sky index k_c is obtained. The clear-sky irradiance models the irradiance measured on a horizontal surface on Earth on a cloudless clear day. To obtain such irradiance, in this work we employed the ESRA model [16]. This index has the same advantages of removing daily cycles and allowing for studying the changes caused by clouds [17].

Following the same logic as for $\sigma(\Delta G)$, variability of irradiance can be described by means of the differences of k_t or k_c by using $V = \sigma(\Delta k_t)$ or $V = \sigma(\Delta k_c)$.

Changes in irradiance can also be quantified in terms of ramps. In other words, how deep the rate of change of irradiance in a period Δt is. Thus, the ramps are defined as (3)

$$r = \frac{\Delta G}{\Delta t} \tag{3}$$

Since ramps are changes, the standard deviation method is also used for quantifying irradiance variability: $V = \sigma(r)$. As discussed above, irradiance with high variability exhibits large changes in a short time and hence higher ramps. The maximum value of the ramps is then used to describe the irradiance variability ($V = \max(r)$). In addition, following the same logic, the mean ramp, instead of the maximum, is studied as an irradiance variability metric (i.e., $V = \mu(r)$).

Finally, the Variability Index (VI) describes the variability of irradiance as a ratio of the length of the ramps of the measured irradiance with the clear-sky irradiance as seen in (4) [18]

$$VI = \frac{\sum \sqrt{\Delta G^2 + \Delta t^2}}{\sum \sqrt{\Delta G_{clear}^2 + \Delta t^2}} \tag{4}$$

1.2. Previous Analyses of P&O under Variable Irradiance

In the study of the P&O performance in changing irradiance, it is worth mentioning the European standard EN50530 for testing the overall efficiency (tracking and converter) of PV inverters [19]. It defines a triangular-like test signal with increasing slopes (from 0.5 to 50 W/m^2/s) and then repeated at a higher base irradiance and with slopes varying from 10 to 100 W/m^2/s. The sequence is used to simulate changes in irradiance.

In [20], the EN50530 was used to compare the performance of the P&O and the incremental conductance algorithms. The efficiency of P&O is lower at low irradiation and slow irradiance changes but lowest with abrupt changes and low irradiance. The reported average efficiency is 98.3%. The EN50530 standard was also used in [21] to compare different P&O methods. The fixed-step (where the magnitude of the voltage perturbations is constant) version of the P&O was used as a reference and multiple versions of the algorithm with variable steps (where the voltage perturbations are not constant while tracking) were tested. Variable-step versions of the P&O provide an improvement in the performance of the algorithm (e.g., [22]).

The performance of the P&O can also be studied using real conditions as done in [11]. The authors ran the algorithm under different sky conditions. The lowest efficiency for the P&O was 96.5% under partly cloudy skies.

Other studies focused on optimizing the parameters of the P&O algorithm—in particular, the magnitude of the perturbation and the time between perturbations. This leads to conditions for avoiding the algorithm from being confused [12], or expressions that relate the efficiency with the perturbation size [23].

The efficiency of the MPPT system consists of two parts: the hardware efficiency and the tracking efficiency of the algorithm [7]. While most of the previous works focus on the total system efficiency, we focused only on the tracking efficiency of the algorithm and studied the algorithm's efficiency when operating at real irradiance. Our assumptions of an ideal converter and uniform irradiance provide the best-operating conditions for the algorithm. Hence, by quantifying the variability of solar irradiance, we can determine the inevitable loss of efficiency of the algorithm's logic.

To achieve this objective, we present the methodology used for our study in Section 2. The results of Section 3 present our observations regarding the relationship between the algorithm efficiency and irradiance variability, the effect of the tuning parameters of the algorithm, and the influence of the PV module's tilt. We provide an extensive discussion of the results in Section 4 before giving our conclusions in Section 5.

2. Materials and Methods

The P&O algorithm performs voltage perturbations with a sampling time (T_a) less than 1 s. Hence, the use of data in the minute range results in rates of irradiance changes that are too slow to yield any conclusion. The larger the data time step, the smoother the rates of change in irradiance. This occurs partly due to the averaging typically performed by the data acquisition systems. For this reason, we used 3-second sampled irradiance data of Oahu, Hawaii from NREL [24]. This dataset is one of the few with such high temporal resolution containing the three components of irradiance: Global Horizontal Irradiance (GHI), Direct Normal Irradiance (DNI), and Diffuse Horizontal Irradiance (DHI). We used these quantities to calculate the irradiance impinging on the same plane as the PV module using Equation (5):

$$G = G_{dir} + G_{diff} + G_{ref} \tag{5}$$

The direct component (G_{dir}) is calculated from the measured DNI and the angle between the Sun and the vector normal to the module. We used the isotropic sky model approach to translate the measured DHI to the plane of the module and calculate the diffuse component (G_{diff}). For the reflected component (G_{ref}), we assumed a constant value for the albedo of 0.2. We will refer to the plane-of-module irradiance simply as "irradiance".

Since the irradiance does not change instantaneously but in a ramping way, we used linear interpolation to connect two consecutive data points with a ramp. Each new point is separated by the sampling time (T_a). At every point, we used the approach proposed by [25], based on the well-known single diode model to obtain power–voltage (P–V) curves. The module is treated as ideal, thus neglecting series and parallel resistances [25]. We used the datasheet of the front side of a 400 W Trina Solar DUOMAX Twin module for fitting the model. Except for Section 3.3, the simulation considered a single, horizontally placed module, uniform irradiance (i.e., no partial shading), and free horizon (i.e., no obstacles in the surroundings). The ambient temperature was kept constant at 25 °C. With this, we ensure that all effects are due to irradiance changes only. For all the interpolated datasets, the P&O algorithm was run to find the maximum power point at each step. To improve our analysis, we only considered irradiance values above 20 W/m^2 that occurred when the elevation of the Sun was greater than 5°.

The baseline sampling time (T_a) of the P&O was set at 50 ms and a voltage step (ΔV) of 0.3 V.

In reality, the power converter performs the MPPT algorithm. However, we decided to consider this component ideal. Then, the sampling time and voltage step are used to simulate the algorithm directly on the P–V curve of the module. We ensure that the algorithm operates under the most favorable conditions by neglecting the power converter and assuming uniform irradiance on the (ideal) module. This allows us to compute the efficiency losses of the logic of the algorithm caused exclusively by irradiance variability.

Since the P&O algorithm swings around the MPP, the efficiency cannot be calculated with a unique power point. Instead, we considered the efficiency as a ratio of energies for a given time period (6) as done by [20]:

$$\eta_{MPP} = \frac{\int_0^{T_M} P_{op}}{\int_0^{T_M} P_{MPP}} \tag{6}$$

where P_{op} is the power output of the module operating under the P&O algorithm at a particular moment. P_{MPP} is the theoretical maximum power point of the module at the same P–V curve. The integrating interval T_M was set at 3-s and 1 min.

The variability of solar irradiance is related to the variance of the measured irradiance, and its quantifiers are mainly based on the standard deviation of differences between measured points. An extended description of the used quantifiers was presented in Section 1.1. The period used for irradiance variability calculations was set at 1 min, using the 3-s sampled data.

3. Results

Here, we present a statistical analysis of the efficiency loss of the logic of the P&O algorithm when it operates under changing irradiance. First, the results explore the relationship between variability and efficiency of the algorithm. Based on the observations, a model that quantifies such a relation is presented. We then move to determine the effects of the tuning parameters before presenting an analysis of the influence of the module tilt. Unless explicitly mentioned in the next sections, the term *efficiency* pertains to the efficiency of the algorithm.

3.1. Impact of Irradiance Variability on the Efficiency of the Algorithm

The efficiency of the P&O algorithm is not constant. It experiences sudden drops when the irradiance changes. The depth and frequency of the efficiency drops lead to dispersion in the obtained efficiency values. In other words, scattered efficiency values

indicate a deeper efficiency decrease. The dispersion can be easily quantified using the standard deviation of the efficiency, $\sigma(\eta_{MPP})$. We related this to the standard deviation of the changes in irradiance, $\sigma(\Delta G)$, as a measure of variability. Figure 2 shows that higher irradiance variability corresponds to higher efficiency dispersion indicating a relation between the two.
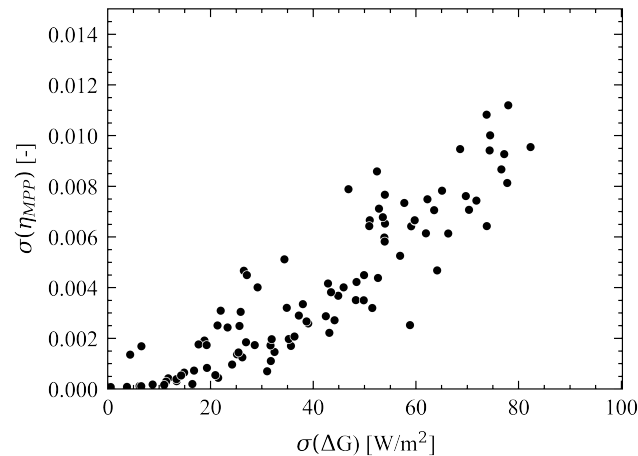
Figure 2. Daily dispersion of differences in irradiance, $\sigma(\Delta G)$, causes increased daily dispersion of the calculated efficiency, $\sigma(\eta_{MPP})$, for 100 randomly selected days. Two outliers were removed for clarity.

Although Figure 2 shows some impact of irradiance variability on efficiency, a Pearson correlation analysis shows a minimal linear correlation between the 1 min irradiance variability and the 1 min efficiency with all variability metrics ($\bar{r} = -0.45$). Note that this correlation is against the 1 min efficiency values and not with the standard deviation of efficiency. A single variability value is not linked to a single efficiency value but many. Because of this, no clear trend can be derived.

To reduce the scattering of the data and obtain a better insight into the effect of irradiance variability on the algorithm's efficiency, the data were grouped into 50 irradiance variability bins. At every bin, efficiency was averaged as well as the irradiance variability (given by $\sigma(\Delta G)$) corresponding to each bin. With this binning approach, we found that the average efficiency $\bar{\eta}_{MPP}$ is related to the mean of irradiance variability, $\overline{\sigma(\Delta G)}$, through the quadratic expression (7):

$$\bar{\eta}_{MPP} = p_1 \bar{V}^2 + p_2 \bar{V} + p_3 \tag{7}$$

where $\bar{V} = \overline{\sigma(\Delta G)}$. The values for the coefficients p_1, p_2, and p_3 can be found in Appendix A.

The proposed model is illustrated in Figure 3. When binning is applied, the model accurately describes the relationship between efficiency and irradiance variability.

Although $\sigma(\Delta G)$ was used as a metric for irradiance variability, other metrics exist to describe irradiance variability, namely,

- Standard deviation of changes of the clearness index;
- Standard deviation of changes of the clear-sky index;
- Standard deviation of ramps;
- Maximum ramp;
- Variability Index.

These were extensively detailed in Section 1.1. To explore the validity of our model for other metrics, we repeated the analysis for the metrics mentioned above, finding that the model can be applied to all of them. This is not unexpected as the studied variability metrics are strongly linearly correlated with each other, with Pearson correlation coefficients exceeding 0.8.
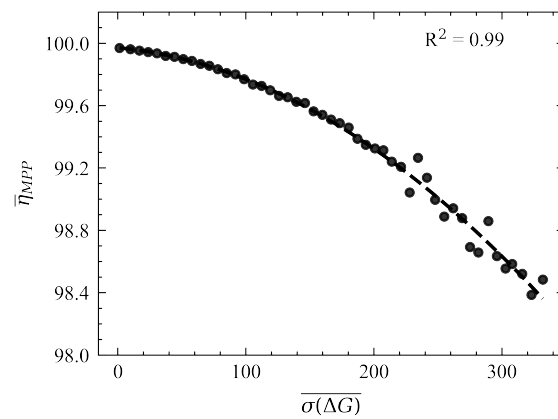
Figure 3. Drop of the binned average efficiency, $\bar{\eta}_{MPP}$, of the P&O algorithm as a function of the mean irradiance variability in each bin, $\overline{\sigma(\Delta G)}$. The coefficient of determination (R^2) is included in the graph to indicate the goodness of fit. Other variability metrics can also be fitted with the model. The fitting parameters are given in Appendix A.

3.2. Sensitivity of the P&O Parameters

We selected 1 h of data at the same timestamp (12:00 p.m. to 1:00 p.m. local time, Oahu, Hawaii) with different irradiance variability. For each hour chosen, we modified the sampling time, T_a, logarithmically between 0.1 and 1000 ms and ΔV linearly from 0.1 to 3% of the open circuit voltage of the module at Standard Test Conditions ($V_{oc(STC)}$). Figure 4a shows the results of this analysis on an hour with low irradiance variability in contrast to an hour with high irradiance variability as in Figure 4b. Under stable irradiance, T_a does not have a significant impact on the P&O performance, and the efficiency loss is mainly determined by ΔV (Figure 4a). With variable irradiance, T_a plays an important role. As both parameters influence the efficiency loss under varying conditions, a poorly tuned algorithm with slower sampling time in combination with significant voltage perturbation can experience losses of up to 2% (Figure 4b).
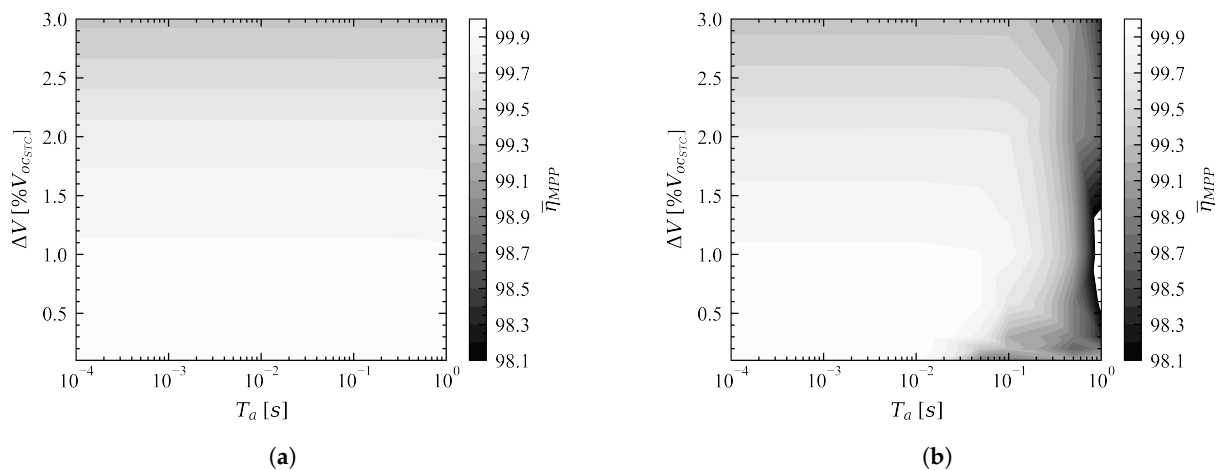
Figure 4. Sensitivity of the P&O algorithm efficiency, η_{MPP}, to its parameters under (**a**) clear skies, and (**b**) variable irradiance.

3.3. Impact of the Module Tilt

So far, our analysis was focused on a horizontally placed module. For a tilted module, the efficiency loss is more significant near the tilt angle of the module that maximizes the annual irradiance ("optimal angle"). More direct irradiance reaches an optimally tilted module than a horizontal one. This implies that a cloud blocking the Sun will cause a more profound reduction of the available irradiance to the module, increasing the effect of

variability. To support this argument, we simulated a module placed horizontally and then gradually increased its tilt in steps of 5° until vertically placed. One randomly-selected highly variable day served as the input for all the angles. The simulation followed the procedure explained in Section 2. Figure 5 shows the dispersion of the P&O algorithm efficiency as the tilt angle increases. The dispersion of efficiency, linked to a more considerable efficiency loss, is higher near the optimal angle for this day. As the module is tilted away from the optimal angle, the direct irradiance exhibits lower peaks. This is linked to lower efficiency losses.
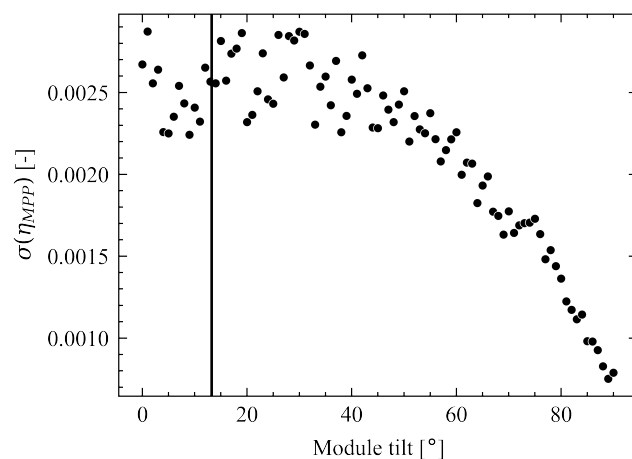
Figure 5. Impact of the module tilt on the daily efficiency for one randomly selected day. For the studied location, the optimal tilt angle is 13.23°, marked with the vertical line.

4. Discussion

We hypothesized that moments with significant changes in irradiance experience the lowest algorithm efficiency. Then, it should be possible to draw a relation between irradiance variability and efficiency. This, curiously, is not a linear relation and also not a simple task to relate the two quantities. Figure 2 only indicates that efficiency data become more spread as the variability of irradiance increases. However, from Figure 2, it is not possible to quantify the efficiency loss. In other words, Figure 2 gives only an indication of the existence of a relation between irradiance variability and efficiency. It is only after the binned efficiency analysis (Figure 3) that we can establish a comprehensive connection between irradiance variability and algorithm efficiency.

When the algorithm gets confused, the operating point will drift away from the MPP. The amount of divergent points depends on the steepness of the irradiance ramp. For shallow ramps of solar irradiance, this drift occurs in one or two points before the algorithm swings back again towards the correct operation. Thus, the impact on efficiency can be neglected. This is not true for steep ramps. Under such conditions, the algorithm diverges during more points, causing substantial drops in the instantaneous efficiency (We observed instantaneous efficiency values dropping as low as 80%). Furthermore, after the algorithm has diverged, it needs additional steps to climb back towards the MPP.

The P&O algorithm's efficiency also depends on its tuning parameters. We observed that, on clear days (Figure 4a), the efficiency drops with large voltage steps. This is in line with the remarks of other authors who observed that increasing the perturbation step leads to better dynamic performance, as the MPP is reached faster, but with the disadvantage of a poor steady state tracking due to the swinging around the MPP [26]. Interestingly, when optimizing the perturbation step, some authors have found voltage perturbations that exceed 2% of their module's V_{oc} [23,27]. In contrast, we observed that the highest dynamic efficiency for clear and highly variable days is obtained with lower voltage steps. For practical MPPTs, the voltage perturbation is below 1% [13].

Regarding the sampling time (T_a), values found in the literature range from 0.05 s to 0.1 s (1–20 Hz) [13,23,28]. Even when these parameters were optimized considering the response of the PV module and the power converter [27], the losses caused by variability only become significant. This is clear from Figure 4b. The range of T_a approached the right half of the figure where efficiency is lower, especially combined with small perturbation steps.

The efficiency values for the P&O algorithm given in the literature span over a broad range. Some of the efficiency values are as low as 62.63% for a test under EN50530 with low irradiance and small perturbation step [29]. Under real conditions, the reported mean efficiency of the algorithm was 98.3% [20]. In [11], and the authors determined that the efficiency under partly cloudy days was 96.5%, while, for a clear day, it was 98.7%.

One possible reason for the large discrepancy in the efficiency values is the integration period that different authors consider for their calculations. All these studies (including the present work) use Equation (6) for the calculation of efficiency. However, the integrating period ranges from a full day to a few seconds.

An additional contribution of this work is the analysis of the impact of the PV module tilt on efficiency. From Figure 5, we see that the scattering of the efficiency reduces as the module is placed more vertically. This is because the variability of irradiance decreases as the module's tilt angle becomes larger. The maximum variability coincides with the optimal angle of the module. Therefore, we can expect a greater efficiency loss at an optimal angle than a horizontally placed module and even greater in comparison with a vertical one. For example, from the data used to obtain Figure 5, we can calculate the irradiance variability $\sigma(\Delta G)$. Using Figure 3, at an optimal angle, the MPPT efficiency is close to 99.90%. We gain 0.02% in tracking efficiency just by placing the module horizontal, and 0.09% for the vertical case.

Another issue worth mentioning is that, in all previous studies, there is a power converter involved, either in simulation or experimental. This can also be a potential reason for the lower values obtained in the literature with respect to our results. The hardware imposes limitations in the study of the logic of the algorithm as the dynamics of the converter, combined with the PV module, determine the optimal parameters of the P&O algorithm [12,27,28]. Additionally, the hardware imposes limitations regarding how fast the PV module can react to a duty cycle change [26,30], which is related to the maximum sampling frequency that can be used for the perturbations [31]. The resolution of the analog-to-digital converters of the control system and the sensitivity of the sensors imposes constraints on the minimum step size that can be employed [27].

In [20], the authors attributed extremely low values of efficiency observed (<95%) during real conditions to poor performance on the converter. In our simulations, we also observed such behavior (efficiency dropping as low as 80%), which suggests that the hardware is not the only one responsible for large drops in irradiance but the logic of the algorithm itself.

Although Figures 4a,b show an idealized situation, in practice, these values could not be reached due to hardware limitations. The importance of our study relies on the fact that the logic of a well-tuned algorithm, under the most favorable conditions for the algorithm (not considering any power electronics and no partial shading), causes a systematic efficiency loss that, on a monthly basis, can reach up to 0.1% due to variable irradiance. This represents a production reduction of approximately 1 h per month at the selected site.

5. Conclusions

We studied the relation of irradiance variability to the efficiency of the P&O MPP tracking algorithm. We found a connection between the binned efficiency and irradiance variability that a second-order polynomial can describe. The confusion of the P&O algorithm depends on the ramps caused by irradiance variability. The divergence of the algorithm results in a systematic decrease in efficiency that can account for up to 0.1% on a monthly average. A wrong choice of the algorithm's parameters and the module tilt

significantly impacts the efficiency on highly variable days. Our study opens the possibility for an efficiency analysis in different locations around the globe with the sole input of global horizontal irradiance as well as to compare newer and more advanced algorithms. A considerable amount of resources is spent on increasing the efficiency of solar cells. As single-junction solar cells are reaching the theoretical limit, even small improvements in efficiency are regarded as a success. The loss caused by irradiance variability in one of the most used MPPT algorithms is on the same order of magnitude as the cell's efficiency improvement, highlighting the importance of properly tuning the algorithm to its operation under rapidly changing weather conditions.

Including this loss into the PV systems analysis can help to reduce uncertainty in energy yield caused by irradiance variability and facilitate the growth of PV for meeting the generations' goals of the Net Zero Scenarios set in 2030.

Author Contributions: Conceptualization, V.A.M.L. and H.Z.; methodology, V.A.M.L. and U.Ž.; validation, V.A.M.L. and U.Ž.; formal analysis, V.A.M.L. and U.Ž.; investigation, U.Ž.; data curation, U.Ž.; writing—original draft preparation, V.A.M.L.; writing—review and editing, U.Ž., H.Z. and O.I.; supervision, H.Z. and O.I.; project administration, M.Z and O.I.; funding acquisition, M.Z. and O.I. All authors have read and agreed to the published version of the manuscript.

Funding: This activity is co-financed by Shell and a PPP-allowance from Top Consortia for Knowledge and Innovation (TKI's) of the Dutch Ministry of Economic Affairs and Climate in the context of the TU Delft e-Refinery program.

Data Availability Statement: The data used for this study were obtained from the *National Renewable Energy Laboratory* [24], and it is publicly available on their website at http://doi.org/10.5439/1052451 (accessed on 2 June 2021).

Conflicts of Interest: The authors declare no conflict of interest. The funders had no role in the design of the study, in the collection, analyses, or interpretation of data, in the writing of the manuscript, or in the decision to publish the results.

Abbreviations

The following abbreviations are used in this manuscript:

MPP	Maximum Power Point
P&O	Perturb-and-Observe
P–V	Power–Voltage
GHI	Global Horizontal Irradiance
DHI	Diffuse Horizontal Irradiance
DNI	Direct Normal Irradiance

Appendix A. Parameters of the Binned Efficiency Model

Table A1 shows the fitting parameters of (7) for different variability metrics for the Oahu dataset and 3-second data. Note that the offset term, p_3, is always close to 99.9 because the expected algorithm efficiency lies within this range.

Table A1. Parameters of the binned efficiency model.

Metric	p_1	p_2	p_3	R^2
$\sigma(\Delta G)$	-1.22×10^{-5}	-8.03×10^{-4}	99.97	0.99
$\sigma(\Delta k_t)$	-28.90	0.61	99.95	0.99
$\sigma(\Delta k_c)$	$-19.63.94$	0.33	99.97	0.97
$\sigma(r)$	-2.50×10^{-4}	2.15×10^{-3}	99.92	0.90
$\max(r)$	0	-2.94×10^{-3}	1.00	0.92
VI	0	-2.98×10^{-4}	99.9	0.92

References

1. Solar, P.V. Technical Report, International Energy Agency. 2021. Available online: https://iea.org/reports/solar-pv (accessed on 21 September 2022).
2. Mittag, M.; Reise, C.; Wohrle, N.; Eberle, R.; Schubert, M.; Heinrich, M. Approach for a Holistic Optimization from Wafer to PV System. In Proceedings of the 2018 IEEE 7th World Conference on Photovoltaic Energy Conversion (WCPEC) (A Joint Conference of 45th IEEE PVSC, 28th PVSEC & 34th EU PVSEC), Waikoloa, HI, USA, 10–15 June 2018; pp. 3194–3199. [CrossRef]
3. Photovoltaics Report. Technical Report, Fraunhofer Institute for Solar Energy Systems. 2022. Available online: https://www.ise.fraunhofer.de/content/dam/ise/de/documents/publications/studies/Photovoltaics-Report.pdf (accessed on 22 September 2022).
4. CSEM-EPFL. *New World Records: Perovskite-on-Silicon-Tandem Solar Cells*; Stanford University: Stanford, CA, USA, 2022.
5. Calcabrini, A.; Muttillo, M.; Weegnik, R.; Manganiello, P.; Zeman, M.; Isabella, O. A fully reconfigurable series-parallel photovoltaic module for higher energy yields in urban environments. *Renew. Energy* **2021**, *179*, 1–11. [CrossRef]
6. Venkateswari, R.; Sreejith, S. Factors influencing the efficiency of photovoltaic system. *Renew. Sustain. Energy Rev.* **2019**, *101*, 376–394. [CrossRef]
7. Karami, N.; Moubayed, N.; Outbib, R. General review and classification of different MPPT Techniques. *Renew. Sustain. Energy Rev.* **2017**, *68*, 1–18. [CrossRef]
8. Kordestani, M.; Mirzaee, A.; Safavi, A.A.; Saif, M. Maximum Power Point Tracker (MPPT) for Photovoltaic Power Systems—A Systematic Literature Review. In Proceedings of the 2018 European Control Conference (ECC), Limassol, Cyprus, 12–15 June 2018; pp. 40–45. [CrossRef]
9. Motahhir, S.; El Hammoumi, A.; El Ghzizal, A. The most used MPPT algorithms: Review and the suitable low-cost embedded board for each algorithm. *J. Clean. Prod.* **2020**, *246*, 118983. [CrossRef]
10. Abdel-Salam, M.; El-Mohandes, M.T.; Goda, M., On the Improvements of Perturb-and-Observe-Based MPPT in PV Systems. In *Modern Maximum Power Point Tracking Techniques for Photovoltaic Energy Systems*; Eltamaly, A.M., Abdelaziz, A.Y., Eds.; Springer International Publishing: Cham, Switzerland, 2020; pp. 165–198. [CrossRef]
11. Hohm, D.P.; Ropp, M.E. Comparative study of maximum power point tracking algorithms. *Prog. Photovoltaics Res. Appl.* **2003**, *11*, 47–62. [CrossRef]
12. Femia, N.; Petrone, G.; Spagnuolo, G.; Vitelli, M. Optimization of perturb and observe maximum power point tracking method. *IEEE Trans. Power Electron.* **2005**, *20*, 963–973. [CrossRef]
13. Sera, D.; Mathe, L.; Kerekes, T.; Spataru, S.V.; Teodorescu, R. On the Perturb-and-Observe and Incremental Conductance MPPT Methods for PV Systems. *IEEE J. Photovoltaics* **2013**, *3*, 1070–1078. [CrossRef]
14. Woyte, A.; Vu Van, T.; Purchala, K.; Belmans, R.; Nijs, J. Quantifying the occurrence and duration of power fluctuations introduced by photovoltaic systems. In Proceedings of the 2003 IEEE Bologna Power Tech Conference, Bologna, Italy, 23–26 June 2003; pp. 1–7. [CrossRef]
15. Liu, B.Y.; Jordan, R.C. The interrelationship and characteristic distribution of direct, diffuse and total solar radiation. *Sol. Energy* **1960**, *4*, 1–19. [CrossRef]
16. Rigollier, C.; Bauer, O.; Wald, L. On the clear sky model of the ESRA—European Solar Radiation Atlas—With respect to the heliosat method. *Sol. Energy* **2000**, *68*, 33–48. [CrossRef]
17. Lave, M.; Kleissl, J.; Stein, J. Chapter 7—Quantifying and Simulating Solar-Plant Variability Using Irradiance Data. In *Solar Energy Forecasting and Resource Assessment*; Kleissl, J., Ed.; Academic Press: Boston, MA, USA, 2013; pp. 149–169. [CrossRef]
18. Stein, J.; Hansen, C.; Reno, M.J. The Variability Index: A New and Novel Metric for Quantifying Irradiance and PV Output Variability. 2012. Available online: https://www.osti.gov/biblio/1068417 (accessed on 25 September 2022).
19. Bründlinger, R.; Henze, N.; Häberlin, H.; Burger, B.; Bergmann, A.; Baumgartner, F. prEN 50530-The new european standard for performance characterisation of PV inverters. In Proceedings of the 24th EU PV Conference, Hamburg, Germany, 21–25 September 2009; pp. 3105–3109.
20. Ishaque, K.; Salam, Z.; Lauss, G. The performance of perturb and observe and incremental conductance maximum power point tracking method under dynamic weather conditions. *Appl. Energy* **2014**, *119*, 228–236. [CrossRef]
21. Chen, P.C.; Chen, P.Y.; Liu, Y.H.; Chen, J.H.; Luo, Y.F. A comparative study on maximum power point tracking techniques for photovoltaic generation systems operating under fast changing environments. *Sol. Energy* **2015**, *119*, 261–276. [CrossRef]
22. Pandey, A.; Dasgupta, N.; Mukerjee, A.K. High-Performance Algorithms for Drift Avoidance and Fast Tracking in Solar MPPT System. *IEEE Trans. Energy Convers.* **2008**, *23*, 681–689. [CrossRef]
23. Kjær, S.B. Evaluation of the "Hill Climbing" and the "Incremental Conductance" Maximum Power Point Trackers for Photovoltaic Power Systems. *IEEE Trans. Energy Convers.* **2012**, *27*, 922–929. [CrossRef]
24. Sengupta, M.; Andreas, A. Oahu Solar Measurement Grid (1-Year Archive): 3-Second Solar Irradiance; Oahu, Hawaii (Data). 2010. Available online: https://midcdmz.nrel.gov/apps/sitehome.pl?site=OAHUGRID (accessed on 2 June 2021).
25. Spertino, F.; Ahmad, J.; Di Leo, P.; Ciocia, A. A method for obtaining the I-V curve of photovoltaic arrays from module voltages and its applications for MPP tracking. *Sol. Energy* **2016**, *139*, 489–505. [CrossRef]
26. Rezk, H.; Eltamaly, A.M. A comprehensive comparison of different MPPT techniques for photovoltaic systems. *Sol. Energy* **2015**, *112*, 1–11. [CrossRef]

27.   Jately, V.; Azzopardi, B.; Joshi, J.; Venkateswaran, V.B.; Sharma, A.; Arora, S. Experimental Analysis of hill-climbing MPPT algorithms under low irradiance levels. *Renew. Sustain. Energy Rev.* **2021**, *150*, 111467. [CrossRef]

28.   Kivimäki, J.; Kolesnik, S.; Sitbon, M.; Suntio, T.; Kuperman, A. Revisited Perturbation Frequency Design Guideline for Direct Fixed-Step Maximum Power Point Tracking Algorithms. *IEEE Trans. Ind. Electron.* **2017**, *64*, 4601–4609. [CrossRef]

29.   Li, X.; Wen, H.; Hu, Y.; Du, Y.; Yang, Y. A Comparative Study on Photovoltaic MPPT Algorithms Under EN50530 Dynamic Test Procedure. *IEEE Trans. Power Electron.* **2021**, *36*, 4153–4168. [CrossRef]

30.   Kermadi, M.; Salam, Z.; Ahmed, J.; Mekhilef, S.; Berkouk, E.M. Assessment of maximum power point trackers performance using direct and indirect control methods. *Int. Trans. Electr. Energy Syst.* **2020**, *30*, e12565. [CrossRef]

31.   Elgendy, M.A.; Zahawi, B.; Atkinson, D.J. Operating Characteristics of the P&O Algorithm at High Perturbation Frequencies for Standalone PV Systems. *IEEE Trans. Energy Convers.* **2015**, *30*, 189–198. [CrossRef]